Available online at www.sciencedirect.com
ScienceDirect
Journal of Power Sources 164 (2007) 252–259
JOURNAL OF POWER SOURCES
www.elsevier.com/locate/jpowsour

A high fuel utilizing solid oxide fuel cell cycle with regard to the formation of nickel oxide and power density

Pedro Nehter *

Fuel Cells Laboratory, Faculty of Mechanical Engineering, Hamburg University of Applied Sciences, Berliner Tor 21, D-20099 Hamburg, Germany

Received 11 April 2006; received in revised form 12 August 2006; accepted 23 August 2006
Available online 1 December 2006

Abstract

Within this study a novel high fuel utilizing (High-uf) SOFC system is presented with special focus on the formation of nickel oxide, system efficiency and the required cell area at a fixed system performance of 1 MW. Within the High-uf SOFC cycle, a second SOFC stack is used to utilize a further part of the residual hydrogen of the first SOFC stack. This could be feasible by using an anode gas condenser, which is implemented between the first and the second stack. This reduces the water fraction of the anode gas and thereby the tendency of nickel oxide formation in case of a further fuel utilization. Thus, a higher total fuel utilization can be reached with the second SOFC stack.

With the High-uf SOFC cycle, the system efficiency is increased by 7%-points compared to the simple atmospheric SOFC cycle. Furthermore, the average cell voltage and the fuel utilization are varied to carry out a first optimization of the stack's power density. The results of this optimization have shown that the required cell area of the simple SOFC cycle can be slightly reduced by decreasing the fuel utilization, whereas the High-uf SOFC cycle shows an opposite effect. Here, the required cell area can be reduced at constant voltages by increasing the fuel utilization. Thus, higher system efficiencies could be reached with the High-uf SOFC cycle by using the same cell area as the simple SOFC cycle and at the same tendency of nickel oxide formation.

A second condenser behind the second SOFC stack could be used to increase the carbon dioxide mass fraction up to 92%. This could be interesting for CO_2-sequestring applications as well.

Keywords: SOFC; Thermodynamic analysis; Nickel oxide; Durability; CO_2-sequestring

1. Introduction

Fuel cell systems have the potential to reduce the fuel consumption, noise and gaseous emissions significantly [1]. The commercialization of fuel cell systems needs further developments in materials, stack power density, stack durability and system design. These issues are strongly related with each other. The choice of electrochemical, thermodynamic and constructive parameters, which influence the system cost, have to be investigated carefully for each specific application and each specific economic boundary condition.

Previous studies have shown that solid oxide fuel cells (SOFC) coupled with gas turbines promise highest system efficiencies [1,2]. This is mainly caused by the comparably low exergetic losses within the SOFC stack [3]. Siemens Westinghouse demonstrated the high durability of an atmospheric (system pressure ≈ 1.3 bar) SOFC system with a performance of 100 kW. The efficiency of such atmospheric SOFC systems mainly depends on the average cell voltage, the electrochemical fuel utilization and the demand of excess air. The fuel utilization is commonly chosen with 85% at Ni–cermet anodes. A further amount in fuel utilization would result in a stronger formation of nickel oxide, which decreases the catalytic activity for the hydrogen oxidation. This effect is partly reversible but has to be avoided to increase availability and durability.

Within this study a high fuel utilizing atmospheric SOFC system is presented with special focus on the formation of nickel oxide, system efficiency and the required cell area at a fixed system performance of 1 MW. This system is compared with a simple atmospheric SOFC system to estimate the benefits in efficiency and required cell area, which is strongly related to the installed stack cost. In this context, simulation models including

* Tel.: +49 40 42875 8789; fax: +49 40 42875 8783.
E-mail address: nehter@aol.com.

0378-7753/$ – see front matter © 2006 Elsevier B.V. All rights reserved.
doi:10.1016/j.jpowsour.2006.08.037

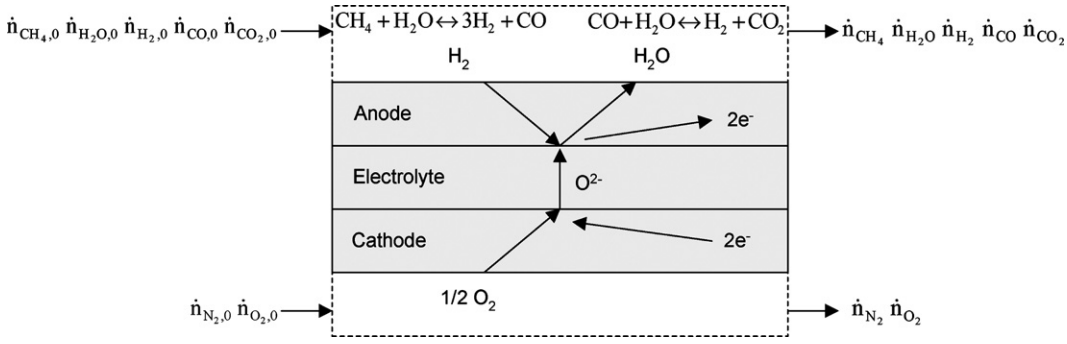

Fig. 1. Control volume.

the SOFC, methane reformer and other system components have been developed within Matlab Simulink.

2. Model

2.1. Fuel processor mode

For the simulation of the fuel processor, the thermodynamic equilibrium is assumed to determine the equilibrium compositions. The chemical species CH_4, H_2, H_2O, CO and CO_2 are taken into account. It is assumed that all gases are ideal fluids. The considered chemical reactions inside the reformer are the steam reforming

$$C_\alpha H_\beta + \alpha H_2O \leftrightarrow \left(\frac{\beta}{2} + \alpha\right) H_2 + \alpha CO$$

and the shift reaction

$$CO + H_2O \leftrightarrow H_2 + CO_2$$

The thermodynamic equilibrium of each reaction is given by

$$\prod x_i^{\nu_i} = \frac{K_p}{p^{\Delta\nu}} = \left(\frac{p^0}{p}\right)^{\Delta\nu} \exp\left(-\frac{\Delta_r G}{RT}\right) \quad (1)$$

where x is the molar fraction of reacting species i, p the absolute pressure, T the absolute temperature, $\Delta_r G$ the free reaction enthalpy, $\Delta_r H$ the reaction enthalpy and $\Delta_r S$ is the reaction entropy. To avoid thermodynamically the carbon deposition (carbon activity < 1), the steam/carbon ratio is chosen with 2.2.

2.2. SOFC model

The thermodynamic equilibrium of the steam reforming and the shift reaction is also used to determine the equilibrium compositions inside the SOFC. At the anode, CH_4, H_2, H_2O, CO, CO_2 and at the cathode, O_2, N_2 are considered as species. The considered reactions inside the SOFC are:

steam reforming :	$CH_4 + H_2O \leftrightarrow 3H_2 + CO$
Shift Reation :	$CO + H_2O \leftrightarrow CO_2 + H_2$
Hydrogen Oxidation :	$H_2 + 0.5O_2 \leftrightarrow H_2O$

The electrochemical oxidation of carbon monoxide is neglected. If the shift reaction fulfills the equilibrium condition, the reversible work of the hydrogen oxidation and carbon monoxide oxidation will have the same value. Investigations of the shift reaction at Ni–cermet anodes have shown [4,5] that the conversions are always close to the equilibrium compositions.

The conversion of the hydrogen and oxygen is determined by Faradays law

$$\dot{n}_{O_2,0} - \dot{n}_{O_2} = \frac{I}{4F}, \qquad \dot{n}_{H_2,0} - \dot{n}_{H_2} = \frac{I}{2F} \quad (2)$$

where the index "0" is used for the molar fraction at the entry of the control volume (Fig. 1).

The electrochemical fuel utilization uf inside a SOFC without any leaks can be calculated by the cell current I and the inlet gas composition:

$$\mathrm{uf} = \frac{I}{F(8\dot{n}_{CH_4,0} + 2\dot{n}_{CO,0} + 2\dot{n}_{H_2,0})} \quad (3)$$

Polarization is a common parameter in the analysis of fuel cell performance. To calculate the relationship between cell voltage U_{Cell} and current density i, a constant area specific resistance $\bar{R}$ is assumed

$$U_{Cell} = U_{Nernst} - \hat{\eta} = U_{Nernst} - \bar{R}i \quad (4)$$

If the electrical performance of the cell P_{el}, the average cell voltage U_{Cell} and the fuel utilization uf are requested parameters, the required cell area is calculated by the average current density $\bar{i}$ as follows:

$$A = \frac{I}{\bar{i}} = \frac{P_{el}}{U_{Cell}} \frac{1}{\bar{i}} \quad (5)$$

The Nernst voltage is considered to be the driving force. It depends strongly on the partial pressures of reactants

$$U_{Nernst} = -\frac{\Delta_r G_{H_2(T,P)}}{2F} = -\frac{1}{2F}\left[\Delta_r G_{H_2(T)} + TR\ln\left(\frac{p_{H_2O}}{p_{H_2}\sqrt{p_{O_2}}}\sqrt{p_0}\right)\right] \quad (6)$$

Thus, the local current density changes along the flow direction of the SOFC. This change is taken into account by the integral of the inverse overpotentials in the following equation:

$$\frac{1}{\bar{i}} = \frac{\bar{R}}{\mathrm{uf}} \int_{uf1}^{uf2} \frac{1}{U_{Nernst(uf)} - U_{Cell}}\,\mathrm{duf} \quad (7)$$

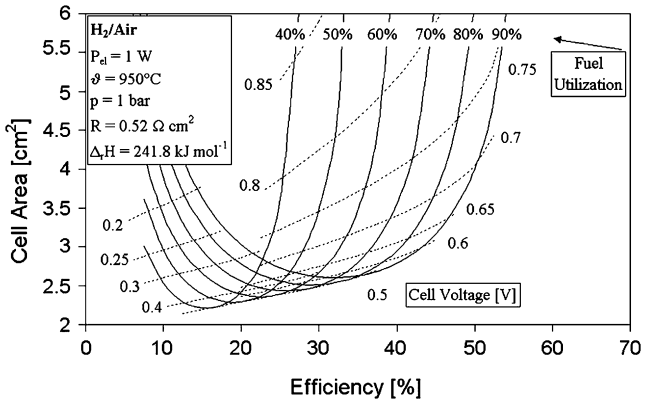

Fig. 2. SOFC area map at design point.

The results of Eq. (5) are shown in Fig. 2. The exemplary required cell area strongly depends on overpotential, fuel utilization and average cell voltage. The efficiency is defined as quotient of the total power and the enthalpy of reaction. The required cell area at a fixed performance decreases with a decreasing cell voltage. As a result the fuel consumption increases due to the lower efficiency of the fuel cell. This is an opposite effect which consists of a design optimum.

2.3. Nickel oxide formation

The formation of nickel oxide at the anode of a SOFC decreases the catalytic activity for the hydrogen oxidation. The formation of nickel oxide is partly reversible but has to be avoided to maximize the long-term stability at high fuel utilization. The oxidation of nickel could occur due to the reaction with H_2O and CO. If the oxidation of hydrogen and carbon monoxide comply the equilibrium condition including the shift reaction, the oxygen activity can be calculated by one of these reactions.

Different models were supposed for the electrochemical oxidation of hydrogen at Ni–YSZ (yttria stabilized zirconia) cermet anodes. The major differences of the models were found with regard to the location where the chemical and electrochemical reactions occur. De Boer suggested that interstitial hydrogen and hydroxyl are formed [7]. Bieberle as well as Mizusaki et al. suggested the presence of adsorbed oxygen on the Ni [6]. Modeling results of the anodic surface coverages of the species O, H, OH and H_2O indicated that the fraction of adsorbed oxygen increases drastically with higher overpotentials [6], which could be an evidence of the formation of NiO at higher overpotentials.

As long as the detailed mechanisms of the hydrogen oxidation and formation of nickel oxide at nickel cermet anodes are not yet clarified, the following assumptions are made for this work. At OCV conditions (open circuit voltage) the formation of NiO can be estimated by the equilibrium activity of the oxygen regarding the H_2O–H_2 ratio of the gaseous phase. In case of operation and non-equilibrium condition at the anode, the potential of the anode (versus air) is displaced to less negative values, mainly caused by the activation overpotential. As a result of the following calculation, the concentration overpotential is lower than 10 mV. Thus, the concentration-dependent change in oxygen activity is considered to have a minor influence on the formation of NiO. The formation of NiO was observed at negative anodic potentials between −850 and −650 mV (versus air) [7], which is the same range of oxygen activity governed by the equilibrium of Ni–NiO system. This is why the anodic potential, calculated by activation and concentration versus air, is used in this work to estimate the formation of NiO.

The formation of nickel oxide is estimated by comparing the anodic potential with the oxygen activity governed by equilibrium of the Ni–NiO system. The equilibrium oxygen activity of $Ni + 1/2O_2 \leftrightarrow NiO$ is calculated by the following equation:

$$\log(a_{O_2})_{Ni-NiO} = 8.96 - \frac{24430}{T} \tag{8}$$

where $p_{O_2,Ni-NiO} = a_{O_2,Ni-NiO} \cdot 1\,\text{bar}$. To avoid the formation of nickel oxide at electrochemical equilibrium condition, it is assumed that the oxygen activity, given by the hydrogen oxidation (Eq. (9)), has to be lower than the oxygen activity of the nickel oxidation (Eq. (8)). The equilibrium of both equations (Eqs. (8) and (9)) were determined by measurements [8]. The oxygen activity of $H_2 + 1/2O_2 \leftrightarrow H_2O$ is given by [8]

$$\log(a_{O_2})_{H_2-H_2O} = 2\log\left(\frac{p_{H_2O}}{p_{H_2}}\right) - \frac{26000}{T} + 5.94 \tag{9}$$

where p_{H_2} is the partial pressure of the hydrogen and p_{H_2O} is the partial pressure of the water. The ratio of these partial pressures is strongly related to the fuel utilization of the SOFC. The results of this empirical approach is similar to those of the thermodynamic equilibrium.

To compare the equilibrium of the Ni–NiO system with the overpotential of an anode, the oxygen activity of the nickel oxidation is converted into a electrical potential related to the potential of a reference air electrode ($p = 1$ bar and $T = T_{SOFC}$). The anode potential versus air is given by

$$\begin{aligned}\Delta U_{An/Air} &= \Delta U^0_{H_2-H_2O/Air} + \hat{\eta}_{An} \\ &= \Delta U^0_{H_2-H_2O/Air} + \hat{\eta}_{Act,An} + \hat{\eta}_{Diff,An}\end{aligned} \tag{10}$$

where η_{An} is the overpotential of the anode, taking the activation (Act) and diffusion overpotential (Diff) of the hydrogen oxidation into account. The calculation of the activation and concentration overpotential is described in the following Sections 2.3.1 and 2.3.2

$$\Delta U^0_{Ni-NiO/Air} = -\frac{RT}{2F}\ln\left(\frac{\sqrt{p_{O_2,Air}}}{\sqrt{p_{O_2,Ni-NiO}}}\right) \tag{11}$$

The equilibrium potential of the anode related to the reference air electrode can be determined by

$$\begin{aligned}\Delta U^0_{H_2-H_2O/Air} &= -\frac{RT}{2F}\ln\left(\frac{\sqrt{p_{O_2,Air}}}{\sqrt{p_{O_2,H_2-H_2O}}}\right) \\ &\approx -\frac{RT}{2F}\ln\left(\frac{K_{p,H_2-H_2O}\, p_{H_2}\sqrt{p_{O_2,Air}}}{p_{H_2O}\sqrt{p^0}}\right)\end{aligned} \tag{12}$$

Fig. 3 shows the tendency of the nickel oxidation (grey area), the potential equivalent of the hydrogen oxidation (dashed lines)

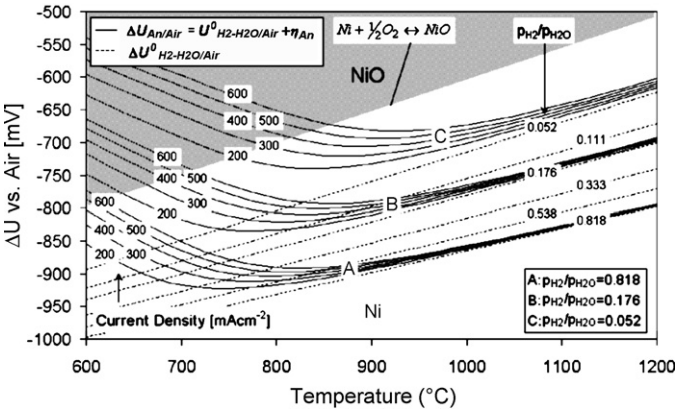

Fig. 3. Anode potential (H_2–H_2O) vs. air (1 bar).

and the anode potential (full lines) as a function of the temperature and p_{H_2}/p_{H_2O} ratio.

The formation of nickel oxide thermodynamically occurs at oxygen pressures higher than 5.9×10^{-11} bar (1000 °C). This partial pressure is equal to an anode potential of −603 mV versus air (1 bar, 1000 °C). Guindet et al. observed an influence on nickel oxide formation at an anode potential, more positive than −800 mV (950 °C) [9]. Therefore, the anode potential is chosen lower than −800 mV in this study. This value is reached at a p_{H_2}/p_{H_2O} ratio of 0.15 (fuel utilization = 85%) and at a temperature of 1000 °C. This is particularly important at the gas outlet of the anode where high fuel utilizations occur. The influence of the activation and diffusion overpotential on the anode potential is comparably small in this range of temperature and fuel utilization. The activation overpotential increases with lower temperatures and the diffusion overpotential increases mainly with lower p_{H_2}/p_{H_2O} ratios.

2.3.1. Local activation overpotential

The activation of a chemical reaction involves energy barriers which must be overcome by the reacting species. These energy barriers are called the activation energy and result in charge transfer polarization. The activation polarization of an electrochemical reaction is usually expressed by the Butler–Volmer equation:

$$i = i_0 \left[\exp\left(\frac{\hat{\alpha} z F \hat{\eta}_{Act}}{RT} \right) - \exp\left(-\frac{(1-\hat{\alpha}) z F \hat{\eta}_{Act}}{RT} \right) \right] \quad (13)$$

where $\hat{\alpha}$ is the transfer coefficient and i_0 is the exchange current density. The transfer coefficient is approximately 0.5 for fuel cells. The exchange current density is the cathodic and anodic electrode reaction rate at the equilibrium potential. A high exchange current density results in a good performance. With $\hat{\alpha} = 0.5$ the activation polarization can be calculated as follows:

$$\hat{\eta}_{Act} = \frac{RT}{0.5zF} \operatorname{arsinh}\left(\frac{i}{2i_0} \right) \quad (14)$$

For the anodic exchange current density of the hydrogen oxidation at Ni–YSZ anodes, Mogensen [10] has proposed the following equation:

$$i_{0,An} = \gamma_{An} \left(\frac{p_{H_2}}{p_{0,An}} \right) \left(\frac{p_{H_2O}}{p_{0,An}} \right) \exp\left(-\frac{E_{Act,An}}{RT} \right) \quad (15)$$

where $E_{Act,An}$ is the activation energy, γ_{An} an empirical pre-exponential factor, p_{H_2} the partial pressure of hydrogen, p_{H_2O} the partial pressure of water and $p_{0,An}$ is the reference pressure at the anode.

2.3.2. Local concentration overpotential

The concentration overpotential at electrodes is a fictive electrical potential drop caused by the concentration difference in the gaseous phase. Diffusion through porous materials is typically described by the binary molecular diffusion and the Knudsen diffusion. In this study, both types of diffusion are taken into account to estimate the concentration overpotential. It is assumed that the concentration gradient along the pore is much higher than the concentration gradient within the surface boundary. Thus, the concentration gradient inside the surface boundary is neglected.

For the ideal gas model the anodic concentration overpotential, which is proportional to the irreversible entropy production, can be written as

$$\hat{\eta}_{Diff,An} = \frac{RT}{zF} \ln\left(\frac{p^*_{H_2}}{p^0_{H_2}} \frac{p^0_{H_2O}}{p^*_{H_2O}} \right) \quad (16)$$

where p^0 is the partial pressure in the gas bulk and p^* is the partial pressure at the end of the pores. The concentration profiles inside the pores can be estimated by using the Fick's law. The molar fraction x can be expressed as

$$x^*_{H_2} = x^0_{H_2} - \frac{RTi\delta_{An}}{p2FD_{eff,An}} \quad (17)$$

$$x^*_{H_2O} = x^0_{H_2O} + \frac{RTi\delta_{An}}{p2FD_{eff,An}} \quad (18)$$

for the equimolar diffusion of hydrogen and water. δ_{An} is here the thickness of the anode and D_{eff} is the effective diffusion coefficient. The effective diffusion coefficient takes the Knudsen diffusion as well as the binary diffusion at the anode into account.

The binary diffusion coefficient between gas species A and B in free space is given by the Chapman–Enskog theory

$$D_{AB} = 1.8583 \times 10^{-6} \left(\frac{1}{M_A} + \frac{1}{M_B} \right)^{1/2} \frac{T^{3/2}}{p\sigma^2_{AB}\Omega_D} \quad (19)$$

where σ is the collision diameter (Lennard–Jones length) and Ω_D is the collision integral based on the Lennard–Jones potential. The collision integral is calculated by the Lennard-Jones energy ε. The Lennard–Jones energy is a function of the critical gas properties and the Boltzmann constant k [11].

The Knudsen diffusion coefficient for a species A is defined as

$$D_{Kn,A} = \frac{2R_{Por}\bar{v}_A}{3} \quad (20)$$

where R_{Por} is the pore radius and $\bar{v}$ is the average velocity of the gas molecule. Both ordinary diffusion and Knudsen diffusion

can be combined within the effective diffusion coefficient which can be written as

$$\frac{1}{D_{\mathrm{eff,Por,A}}} = \frac{\tau_\mathrm{p}}{\theta}\left(\frac{1}{D_{\mathrm{AB}}} + \frac{1}{D_{\mathrm{Kn,A}}}\right) \tag{21}$$

The tortuosity τ_p and porosity θ are used to account the geometry of the pores and relation between solid space and pore space of the electrode.

If the presence of other species except hydrogen and water inside the anodic pores is neglected, the anodic effective diffusion coefficient can be expressed for the ideal gas-mixture as [12]:

$$D_{\mathrm{eff,An}} = \left(\frac{p_{\mathrm{H_2O}}}{p_{\mathrm{ges}}}\right) D_{\mathrm{eff,Por,H_2}} + \left(\frac{p_{\mathrm{H_2}}}{p_{\mathrm{ges}}}\right) D_{\mathrm{eff,Por,H_2O}} \tag{22}$$

(Table 1) lists the assumptions which are made for the previous estimation of the anodic overpotentials.

Table 1
Anode parameters

Thickness anode (Ni–YSZ) (m)	50×10^{-6}
Pre-exponential coefficient for i_0 (A m^{-2})	18.9×10^{9}
Activation energy anode (kJ mol^{-1})	120
Pore radius (m)	0.5×10^{-6}
Tortuosity	6
Porosity (%)	30

3. System configuration

3.1. Simple SOFC cycle

The configuration of the simple SOFC cycle with a performance of 1000 kW is shown in Fig. 4. The simulation is based on the solution of the energy and the mass balances calculated within Matlab Simulink. The model of each component consists of a mode for design studies and a off-design mode which takes the part load characteristics of the fuel cell, the turbo machinery, the pumps and the heat exchangers into account.

The thermodynamic equilibrium Eq. (1) is used to solve the mass balance of the reformer for a predicted outlet temperature. In the reformer the hydrocarbons are converted to H_2, H_2O, CO, CO_2 and residual CH_4 by combining the steam reforming and the shift reaction. For the SOFC stack a constant outlet gas temperature of 1000 °C is chosen. To fulfil the energy balance of the SOFC stack, the inlet temperatures of the SOFC stack is calculated iteratively for a requested total excess air ratio. That involves a partial preheating of the reactants inside stack.

The air is preheated in the heat exchanger (2b) and in a stack integrated heat exchanger to reduce the excess air demand. In the combustor (6a) the methane, hydrogen and carbon-monoxide of the anode gas is oxidized to use the residual heat. The evaporator (1b) is implemented in the exhaust gas stream.

With the listed assumptions (Table 2) the simple SOFC cycle reaches an electrical efficiency of 53% (LHV) at a system pressure of 1.27 bar, an average cell voltage of 0.7 V and an electrochemical fuel utilization of 85%.

3.2. High-uf SOFC cycle

The configuration of the high fuel utilizing (High-uf) SOFC cycle with a performance of 1000 kW is shown in Fig. 5. This system consists of an additional SOFC stack which is connected in series with the first SOFC stack. The second SOFC stack is supplied by the cathode gas of the first SOFC stack after it passed

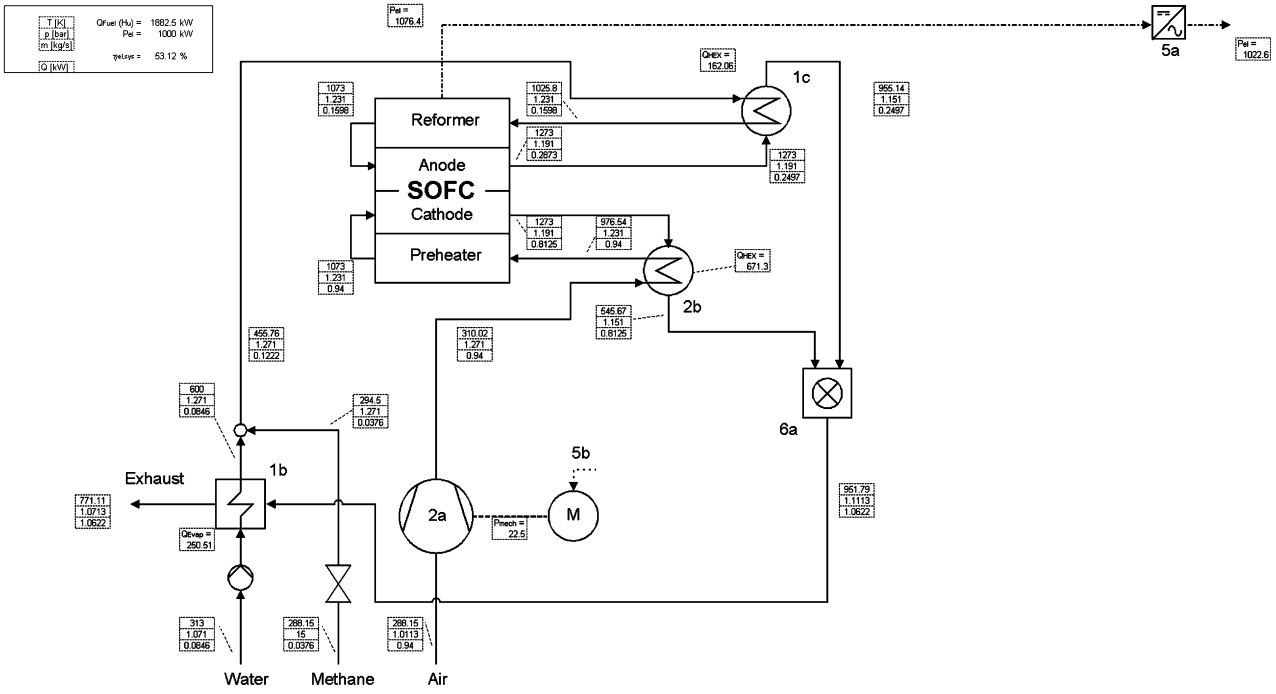

Fig. 4. Simple atmospheric SOFC cycle.

Table 2
Initial parameters of simple SOFC cycle

SOFC average cell voltage (V)	0.7
Fuel utilization (%)	85
SOFC temperature gas outlet (K)	1273.15
System pressure (bar)	1.27
Air ambient conditions (dry air)	288 K, 1.011 bar
Total excess air ratio	1.44
Steam/carbon ratio	2.2
Isentropic efficiency of blower (%)	87
Mechanical efficiency of blower (%)	95
Pressure drop SOFC, HEX, combustor (bar)	0.04; SOFC: 0.01
Thermal losses SOFC, HEX, combustor (%)	0
Inverter efficiency (%)	95
Motor efficiency (%)	96

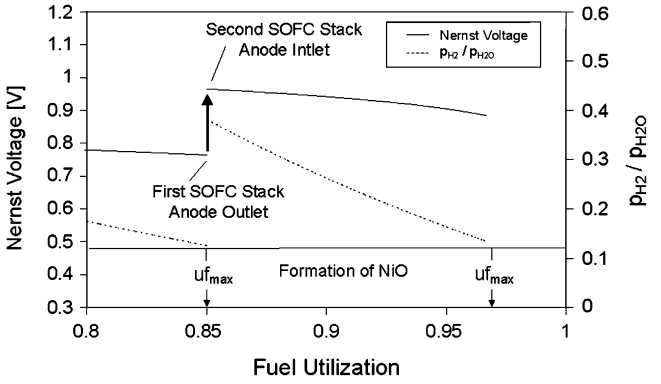

Fig. 6. Nernst voltage vs. fuel utilizations.

the air preheater (2b). The anode gas of the first SOFC stack is led through the regenerative heat exchanger (1d) and the condenser (1e) before it enters the second SOFC stack. The fuel utlization of the first SOFC stack is chosen with 85%. This is equal to the fuel utilization of the simple SOFC cycle. The second SOFC stack is used to increase the fuel utilization up to 97% at an average cell voltage of 0.7 V. It is assumed that the maximum fuel utilization is limited by the p_{H_2}/p_{H_2O} ratio of partial pressures at the outlet of the anode (Section 2.3). The first stack reaches a p_{H_2}/p_{H_2O} ratio of 0.12 and a local Nernst voltage of 0.77 V at the anode outlet (Fig. 6). Within the condenser (1e) the partial pressure of the water is reduced. Thus increases the p_{H_2}/p_{H_2O} ratio up to 0.46 at the condenser outlet (1e). If the equilibrium condition of the shift reaction is taken into account, the reaction will generate water and carbon monoxide by consuming hydrogen and carbon dioxide at the inlet of the second SOFC stack. If the shift reaction complies their equilibrium, the p_{H_2}/p_{H_2O} ratio will decrease again and a Nernst voltage of 0.94 V at the inlet of the second SOFC stack (Fig. 6) is reached. With this p_{H_2}/p_{H_2O} ratio it is feasible to carry out a further fuel utilization without an amount in nickel oxide formation. The fuel utilization of the first and the second SOFC stack increases to 97% in sum when the p_{H_2}/p_{H_2O} ratio (0.12) reaches the same value as the first SOFC stack. Another advantage of this configuration is the amount in

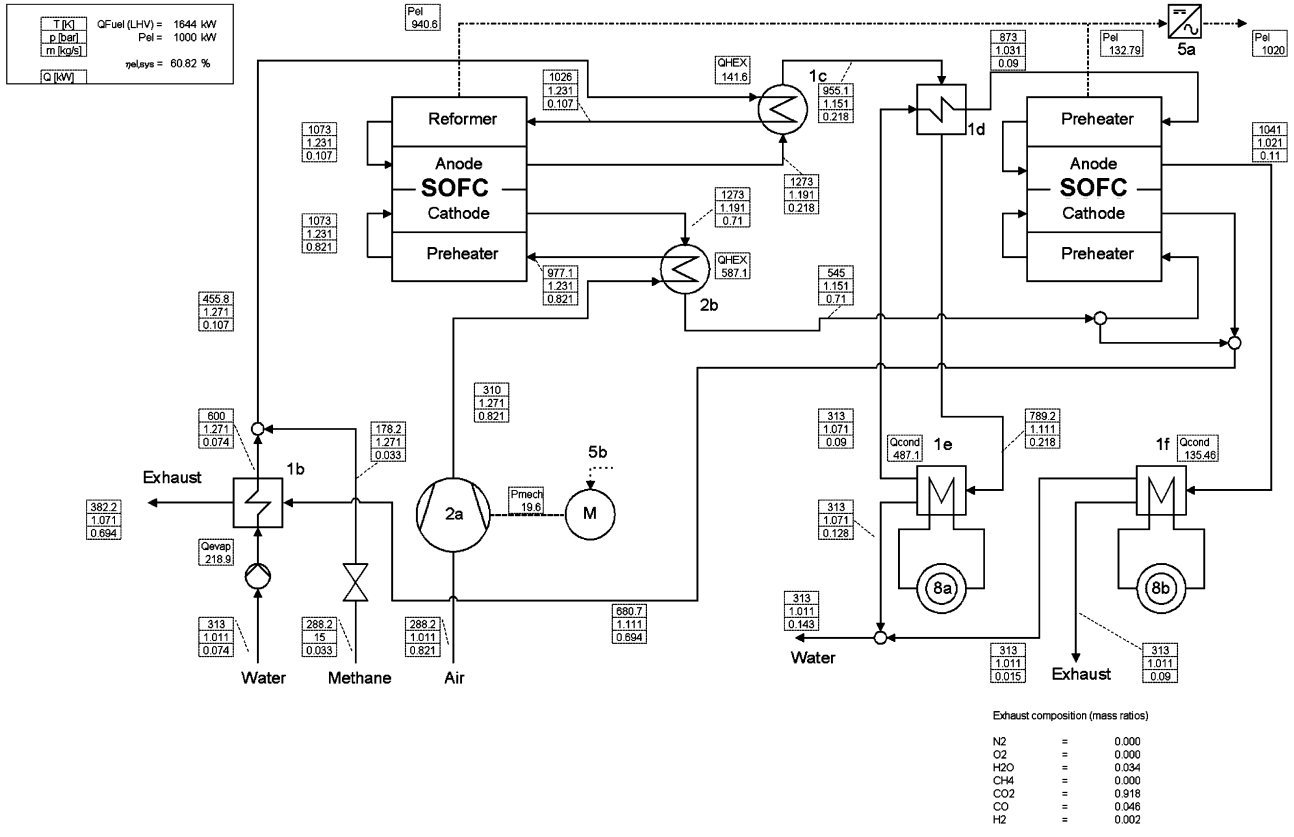

Fig. 5. High-uf atmospheric SOFC cycle.

power density which is due to the higher Nernst voltage at the second SOFC stack inlet. Furthermore, the second condenser (1f) increases the carbon dioxide mass fraction to 92%, which could be interesting for CO_2-sequestring applications. High carbon dioxide mass fractions reduce the energy consumption of the CO_2 storage.

The High-uf SOFC cycle reaches an electrical efficiency of 60% (LHV) at a system pressure of 1.27 bar, an average cell voltage of 0.7 V and a total electrochemical fuel utilization of 97%.

As mentioned before, the steam/carbon ratio is chosen above 2 to avoid carbon deposition. This ratio is reduced within the condenser 1e. Even if the methane is approximately complete converted in the reformer and the first SOFC stack and no carbon deposition is expected from that specie, the Boudouard reaction could result in carbon deposition, especially at low temperatures. This issue is similar to the effort, supplying a PEFC by the anode gas of a SOFC. For this particular configuration, a shift reactor, located between the SOFC and the PEFC, is used to convert the residual carbon monoxide and water into carbon dioxide and hydrogen. A side effect of the shift reaction is, that the carbon activity due to the Boudouard reaction is reduced in that case. This could also become necessary for the proposed "High-uf SOFC cycle", if a carbon deposition occurs in the condenser 1e.

3.3. Required cell area

To compare these two SOFC configurations, the required cell area (Eq. (5)) is estimated at a constant average cell resistance of 0.92 Ω cm^2. The reference case of optimization is chosen at $U_{Cell} = 0.7$ V, uf = 85% of the simple SOFC cycle. The system efficiency is defined as

$$\eta_{el,sys} = \frac{P_{el,sys}}{\dot{n}_{CH_4,sys}\,LHV} \tag{23}$$

where $P_{el,sys}$ is the system performance, $n_{CH_4,sys}$ the molar methane consumption of the system and LHV is the molar lower heating value of the methane. It can be shown that the total electrical current (Eq. (5)) of parallel cells, is also influenced by the requested system's performance and the system's efficiency

$$I = \mathrm{uf}\,F8\dot{n}_{CH_4,sys} = \mathrm{uf}\,F8\frac{P_{el,sys}}{\eta_{el,sys}\,LHV} \tag{24}$$

Eqs. (5) and (24) are used to calculate the change in required cell $A_{SOFC}/A_{SOFC,0}$ at a constant average cell resistance and a fixed system performance of 1 MW.

$$\frac{A_{SOFC}}{A_{SOFC,0}} = \frac{\eta_{el,sys,0}}{\eta_{el,sys}}\frac{\mathrm{uf}}{\mathrm{uf}_0}\frac{\bar{i}_0}{\bar{i}} \tag{25}$$

Fig. 7 shows the influence of the fuel utilization and the average cell voltage on the change in the total required cell area of the simple SOFC cycle (doted lines) and the High-uf SOFC cycle (full lines). The fuel utilization of the simple SOFC cycle is varied from 65% to 85%. For the High-uf SOFC cycle the fuel utilization of the first SOFC stack is kept constant (85%).

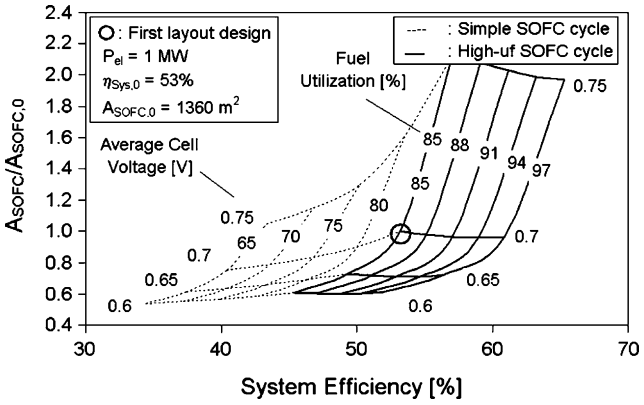

Fig. 7. Influence of U and uf on the required cell area.

The total electrochemical fuel utilization is varied from 85% to 97% with the second stack. Fig. 7 shows that the same system efficiency can be reached with different combinations of cell voltage and fuel. Depending on this combination (U_{Cell}, uf) the thermodynamic parameters of the process and the required cell area are changing.

The average cell voltage of the SOFC is varied from 0.6 to 0.75 V. The required cell area of the simple SOFC cycle can be slightly reduced by decreasing the fuel utilization because the average power density of the stack increases with lower fuel utilizations (Fig. 8). The required cell area of the High-uf SOFC cycle shows an opposite effect. Here, the required cell area can be reduced at constant voltages by increasing the fuel utilization. This is mainly caused by the amount in system efficiency and average power density of the second stack (Fig. 8). The high hydrogen fraction at the inlet of the second stack increases the power density significantly. In case of the High-uf SOFC cycle the influence of the system efficiency on the area reduction is stronger than the influence of the fuel utilization on the area increment.

The average power density of the fuel cell (Fig. 8) is calculated by the stack's total power and the total required cell area at a constant average cell resistance of 0.92 Ω cm^2.

With the presented High-uf SOFC cycle the system efficiency can be increased significantly by using the same cell area as the simple SOFC cycle. This could reduce the installed stack cost at a fixed system performance.

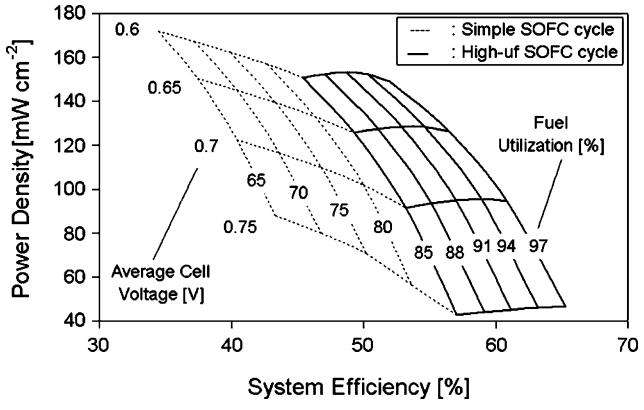

Fig. 8. Influence of U and uf on the average power density.

4. Conclusion

Within this study a high fuel utilizing atmospheric SOFC system is presented with special focus on the formation of nickel oxide, system efficiency and the required cell area at a fixed system performance of 1 MW. In the High-uf SOFC cycle, a second SOFC stack is used to utilize a further part of the residual hydrogen of the first SOFC stack. This is feasible because the tendency of nickel oxide formation at the anode decreases with a lower water fraction. To reduce the water fraction of the anode gas, a condenser is implemented between the first and the second stack. With this configuration, a system efficiency of 60% is reached at a total (first and second stack) electrochemical fuel utilization of 97% and an average cell voltage of 0.7 V. This is 7%-points higher than the efficiency of the simple atmospheric SOFC cycle.

To compare these two configurations, the required cell area is calculated. The required area gives an idea of the expected change in stack cost and stack weight, respectively. Furthermore, the average cell voltage and the fuel utilization are varied to carry out a first optimization of the stack design. The starting point of this optimization is chosen at an average cell voltage of 0.7 V and a fuel utilization of 85%. For the High-uf SOFC cycle the fuel utilization of the first SOFC stack is kept constant (85%). The total electrochemical fuel utilization is varied from 85% to 97% with the second stack. The results of this optimization have shown that the required cell area of the simple SOFC cycle can be slightly reduced by decreasing the fuel utilization, whereas the High-uf SOFC cycle shows an opposite effect. Here, the required cell area can be reduced at constant voltages by increasing the fuel utilization. Commonly, the required cell area increases with an increasing average cell voltage and an increasing fuel utilization. But in case of the High-uf SOFC cycle the influence of the efficiency on the area reduction is stronger than the influence of the fuel utilization on the area increment. With the presented High-uf SOFC cycle the system efficiency can be increased significantly by using the same cell area as the simple SOFC cycle.

A second condenser behind the second SOFC stack can be used to increase the carbon dioxide mass fraction up to 92%. This could be interesting for CO_2-sequestring applications.

Compared to the simple SOFC cycle, it is conceivable that the High-uf SOFC reduces the system cost as long as the cost of the additional heat exchanger and condenser is lower than the savings in stack cost. Furthermore, the increment in system efficiency allows higher system cost. But this depends strongly on the application.

Future work will involve more detailed considerations of the high fuel utilizing stack with regard to the local temperature and current distribution of the cell.

References

[1] W. Winkler, Brennstoffzellenanlagen, Springer-Verlag, 2003.
[2] P. Nehter, W. Winkler, System Analysis of Fuel Cell APUs for Aircraft Applications, H_2-Expo, Hamburg, 2005.
[3] P. Nehter, Thermodynamische und ökonomische Analyse von Kraftwerksprozessen mit Hochtemperatur-Brennstoffzelle SOFC, Shaker Verlag, Dissertation 2005.
[4] J. Metzger, Siemens AG: Untersuchung der Stoffumsätze an mit Methan betriebenen Festelektrolyt-Brennstoffzellen, 1998.
[5] T. Takeguchi, Y. Kani, T. Yano, R. Kikuchi, K. Eguchi, K. Tsujimoto, Y. Uchida, A. Ueno, K. Omoshiki, M. Aizawa, J. Power Sources 112 (2002) 588–598.
[6] A. Bieberle, The electrochemistry of solid oxide fuel cell anodes: experiments, modeling and simulations, Dissertation, 2000.
[7] B. de Boer, SOFC anode, hydrogen oxidation at porous nickel and nickel/yttriastabilised zirconia cermet electrodes, 1998. www.matsceng.ohio-state.edu/ims/BDB.pdf.
[8] Rüdiger Dieckmann, Punktfehlordnung, Nichtstöchiometrie und Transporteigenschaften von Oxiden der Übergangsmetalle Kobalt, Eisen und Nickel, Fachbereich Chemie der Universität Hannover, Habilitationsschrift, 1983.
[9] J. Guindet, C. Roux, A. Hammou, Proceeding of the 2nd SOFC Symposium, Luxembourg, 1991.
[10] M. Mogensen, T. Lindegaard, Riso National Laboratory: Third International Symposium on Solid Oxide Fuel Cells, The Electrochemical Society Proceedings, 1993, p. 484.
[11] P.D. Neufield, A.R. Janzen, R.A. Aziz, J. Chem. Phys. 57 (1972) 1100.
[12] S.H. Chan, K.A. Khor, Z.T. Xia, J. Power Sources 93 (2001) 130–140.